University of Thi-Qar Journal of Science (UTsci)
ISSN Onlin:2709-0256, ISSN Print: 1991-8690 Volume (8), No.2,Oct.2021

Deep Ultraviolet BGaN Quantum Dot structures

Yasmeen Saad
Nassiriya Nanotechnology Research Laboratory (NNRL)/ Science College/ Thi-Qar University
Nasiriyah/ Iraq.
Yasameen_saa.ph@sci.utq.edu.iq

Amin Habbeb AL-Khursan
Nassiriya Nanotechnology Research Laboratory (NNRL)/ Science College/ Thi-Qar University
Nasiriyah/ Iraq.
ameen_2all@yahoo.com.

***Abstract*— This research studies boron-containing quantum dot (QD) structures that emit the ultraviolet. Ternary and quaternary lattice-matched structure: $BGaN/AlN$, $BGaN/BAlN$, $BGaN/AlGaN$, $BAlGaN/AlGaN$, $BAlGaN/BAlN$, $BInGaN/AlN$, $BInGaN/AlGaN$, and $BInAlN/BGaN$ and their TE and TM gain spectra, spontaneous emission, spontaneous polarization, and piezoelectric polarization have been examined in these structures. They have high TE and TM spectra under reducing boron content in the QD or barrier layer. The total polarization decreases for the Al-containing systems, which is preferred. Binary systems emit at 199nm, while the quaternary $BInAlN/BGaN$ can have a peak wavelength near 235nm. Elongating of the wavelength to 290nm is possible with $BInGaN/AlGaN$ with high gain at a few boron contents.**

Keywords: $BGaN$, TE and TM gain, spontaneous emission, spontaneous polarization, and piezoelectric polarization.

I. INTRODUCTION

The ultraviolet (UV) region covers the 10-400 nm wavelength range and enters various applications. For example, non-thermal technology is the most used for food to protect and prolong its shelf life [1]. The deep ultraviolet (DUV) radiation can efficiently kill viruses and bacteria, so they are used in bio-medicine, water, and air purification. Other applications include high-density storage data, medical health care, fluorescence spectroscopy, photolithography [2, 3], and optical lithography with improved resolution [4]. These subwavelengths obtained by semiconductor structures, such as Si, TiO_2, and GaN, crystals can work in infrared and visible regions [5].

AlGaN-based light-emitting diodes have gained significant importance in the UV region and especially in the DUV. Although increasing AlGaN devices performance due to the quality development and devices optimization, it still suffers from higher performance improvement obstacles [3]. It's lattice-mismatched with AlN and GaN substrates cause an internal field in the active region, reducing the carrier recombination as the electrons and holes are spatially separating by this field [6]. So, the required carrier density for optical gain increases for two reasons: first, the leakage by the internal field. Second, the effective hole mass is heavier than the conventional zinc blende crystals such as GaAs and InP. Then, the oscillator strength is degrading, and the emission wavelength is redshifted [7].

AlGaN suffers from poor emission efficiency in the TE mode, the favoring mode in the conventional light-emitting diodes [8]. At high Al content (x ⩾ 0.25), the topmost valence band is the crystal field split-off hole band, a P_z-orbital-like band. Then AlGaN emits in a TM mode which is perpendicular to the c-axis [9].

There are many treatments; the non-(0001) structures (the 0001 is the z-axis or the c-axis in the wurtzite crystals) which can expect to be zero field orientation [7], Kim et al. have enhanced the efficiency by sidewall emission to extract TM DUV light from MQW [9]. There is another development of AlGaN yield by removing the lattice mismatching as closely as possible by using boron [10].

Boron-based devices are proved as a candidate promising for UV and DUV applications. The lattice matching is possible for the structure of these devices with small boron content (<12%). It experimentally demonstrates that up to 9 and 13% boron contents for BGaN and BAlN, respectively, have lattice matching to AlN. Bandgap engineering for the quaternary is possible for wide bandgap BAlGaN structures [2, 10].

Park and Ahn have shown that BAlGaN can work as a UV source with high efficiency and reduced strain [3]. They also have investigated the TM emission increment from this structure [8]. Park refers that boron in BAlGaN QW improves the TE spontaneous emission [2]. Park et al. have compared the emission characteristics from polar (c-plane) and nonpolar (a-plane) BInGaN QW and show that they have higher emission characteristics than InGaN structures [11]. This research studies BGaN, BAlGaN, BInGaN QDs and obtaining high TE and TM gain and spontaneous emission at 199-290nm wavelengths. The result is important in LED work which is not attaining with quantum well (QW) counterpart.

II. BORON-BASED QD STRUCTURES

Many BGaN-based structures have been examined in this work. They are BGaN, BAlGaN, and BInGaN. The parameters were calculated by the following relation [12],

$$P(A_{1-x-y}B_xC_yD) = (1-x-y)P(AD) + x\,P(BD) + y\,P(CD) + x(1-y)P(AD) \quad (1)$$

Where P is any parameter ($E_{gd}, m_e, m_{hh}, a, e_{31}, e_{33}, c_{13}$, c_{33}, and Sp) under examination. This equation is applied to calculate ternary structure these parameters: E_{gd}, m_e, m_{hh}, a, e_{31}, e_{33}, c_{13}, c_{33}, and Sp which are the bandgap, electron and hole effective masses, lattice constant, piezoelectric tensor e_{ij} components, and elastic stiffness components in $B_xAl_yGa_{1-x-y}N$ and $B_xIn_yGa_{1-x-y}N$ from GaN, BN, AlN, and InN binary structures.

III. GLOBAL QUASI-FERMI LEVELS, GAIN, AND SPONTANEOUS EMISSION

In order to account for shape imperfections and random distribution in QDs during their production, the inhomogeneous broadening of the QDs spectrum must be considered. Thus, the optical gain and the spontaneous emission rate can be defined by [13, 14, 15],

$$g_{\sigma}^{tr}(\hbar w) = \frac{\pi e^2}{n_r c \varepsilon_0 m_0^2 w}\sum_i \int d\acute{E}|M_{env}|^2 |\hat{e}.\vec{p}_{cv}|^2 \, D(\acute{E}) L_g(\acute{E},\hbar w)\, f_c(\acute{E},F_c) - f_v(\acute{E},F_v) \qquad (2)$$

The terms f_c and f_v are the respective quasi-Fermi distribution function for the conduction and valence bands, respectively, F_c and F_v are the quasi-Fermi levels of the conduction valence bands. For accurate calculations, take into account the contributions of both the WL and QD layers to the definition of the global quasi-Fermi levels. $|\hat{e}.\vec{p}_{cv}|$ is the momentum matrix element for electron-heavy hole transition energy.

The scripts $m_0, \varepsilon_0, c, n_r, \acute{E}, M_{env}$ are the free mass of electrons, the free space permittivity, the light speed, the material background refractive index, the optical transition energy, and the overlap between envelope functions of the QD electron and hole states, respectively. The term $|\hat{e}.P_{cv}|^2 = \frac{3}{2}(m_0/6)E_p$ is the momentum matrix element for electron-heavy hole transition energy in TE polarization E_p is the optical matrix energy parameter. Express the inhomogeneous state density of self-assembled QDs $D(E')$ as [16]

$$D(\mathrm{E}') = \frac{s^i}{V_{dot}^{eff}} \frac{1}{\sqrt{2\pi\sigma^2}} \exp\left(\frac{-(\mathrm{E}'-\mathrm{E}_{\max}^i)^2}{2\sigma^2}\right) \qquad (6)$$

The degeneracy number at each QD state is for the ground state $s^i = 2$ while for the excited state $s^i = 4$. The factors V_{dot}^{eff}, σ, $E_{\max}^i$ are the QDs effective volume, the spectral variance of the QD distribution, and the transition energy at the maximum QD distribution of the ith optical transition. For accurate calculations, consider the contributions of both the barrier have been considered, the WL, and the QD layers, That was contributed in definition of the global quasi-Fermi levels of the conduction F_c, and valence bands F_v. They were determined from the surface carrier density per QD layer as follows [13];

$$n_{2D} = N_D \sum_i \frac{s^i}{\sqrt{2\pi\sigma_e^2}} \int dE_c' e^{-(E_c'-E_{ci})/2\sigma_e^2} f_c(E_c',F_c) + \sum_l \frac{m_e^* K_B T}{\pi h^2} \ln(1+e^{(F_c-E_{cl})/K_B T}) + \tau_b \frac{1}{2\pi^2}\left(\frac{2K_B T m_{eb}^*}{h^2}\right)^{\frac{3}{2}} e^{\left(\frac{F_c-E_{cb}}{K_B T}\right)} \qquad (7)$$

$$p_{2D} = n_{2D} + N_A^-$$

$$p_{2D} = N_D \sum_i \frac{s^i}{\sqrt{2\pi\sigma_h^2}} \int dE_h' e^{-(E_h'-E_{hi})/2\sigma_h^2} f_v(E_h',F_v) + \sum_m \frac{m_{hh}^* K_B T}{\pi\hbar^2} \ln(1+e^{(F_v-E_{vm})/K_B T}) + \tau_b \frac{1}{2\pi^2}\left(\frac{2K_B T m_{hhb}^*}{\hbar^2}\right)^{\frac{3}{2}} e^{\left(\frac{F_v-E_{hhb}}{K_B T}\right)} \qquad (8)$$

The surface densities of the electrons and holes per QD layer are, respectively, n_{2D} and p_{2D}. The conduction and valence band energies are E_c', E_h'. The respective confined QD state in the conduction and valence bands are E_{ci} and E_{hi}, The spectral variance of QD electron and heavy hole distributions are σ_e and σ_h. The effective electron (hole) mass in the WL and the barrier are, respectively, and $m_{eb}^*(m_{hhb}^*)$. The subband edge energies of the conduction (valence) band in the WL and the barrier are $E_{cl}(E_{vm})$ and $E_{cb}(E_{hhb})$. The term τ_b is the thickness of the barrier and $L_g(E', \hbar\omega)$ is the Lorentzian line shape function of the optical gain and is given by [16];

$$L_g(\mathrm{E}',\hbar\omega) = \frac{1}{\sqrt{2\pi\sigma^2}} \exp\left(\frac{-(\mathrm{E}'-\hbar\omega)^2}{2\sigma^2}\right) \qquad (9)$$

The number of photons emitted per second per unit volume per unit energy is the spontaneous emission rate, R_{sp}, that was calculated from the relation [14, 15],

$$R_{sp} = \frac{n_r^2 w^2}{\hbar\pi^2 c^2} \frac{(2.g_{sp}^{TE} + g_{sp}^{TM})}{3} \qquad (10)$$

In the case of spontaneous emission, the factor $f_c(\acute{E},F_c) - f_v(\acute{E},F_v)$ is replaced by [12, 15],

$$f_c(\acute{E},F_c)[1 - f_v(\acute{E},F_v)]$$

IV. TM MODE MOMENTUM MATRIX ELEMENT OF QD STRUCTURE

The momentum matrix element term $|\hat{e}.p_{cv}|$ of QDs in Eq. (1) depends on the light polarization. The TM polarization momentum matrix element in electron-heavy hole $(e-hh)$ transition is important for the boron-based structures. The TM momentum matrix element of QDs is [12],

$$\left\langle |\hat{e}.p_{e-hh}|^2 \right\rangle = \frac{1}{2\pi}\int_0^{2\pi} d\phi |\hat{z}.p_{e-hh}|^2 = \frac{3}{2} M_b^2 \sin^2\theta \qquad (11)$$

The angular factor $\cos^2\theta$ can be related to the electron or hole wave vectors in the y-direction as follows [17],

$$\cos^2\theta = \frac{E_{cym}}{E_{cnml}} \qquad (12)$$

The CB energy in the y-direction is E_{cym} while E_{cnml} is that of the QD state. As a result, the TM mode momentum matrix elements of the QD structure becomes [18],

$$\left\langle \left| \hat{e}.p_{e-hh} \right|^2 \right\rangle = \frac{3}{2}(1-\cos^2\theta)M_b^2 = \frac{3}{2}(1-\frac{E_{cym}}{E_{cnml}})M_b^2 \quad (13)$$

The bulk momentum matrix element is $M_b^2 = (\frac{m_o}{6})E_p$.

V. Polarization Effects

hh The sum of the spontaneous polarization in the structure, which is at equilibrium, and the piezoelectric polarization δP that results from strain-induced polarization is the total macroscopic polarization (P) of the solid in the absence of external fields. The piezoelectric polarization is proportional to the strain ϵ in the linear regime [19],

$$\delta P_i = \sum_j e_{ij}\ \epsilon_j \quad (14)$$

The equation (14) specifies the piezoelectric tensor components e_{ij} (using Voigt notation). Since the (0001) axis is the growth direction of both bulk materials and nitride superlattices, the polarization is considering along this direction. The piezoelectric polarization is simply expressing as [19],

$$P_{PZ} = 2\frac{a-a_0}{a_0}\left(e_{31} - e_{33}\frac{c_{13}}{c_{33}}\right) \quad (15)$$

where a_0 is the equilibrium value of the lattice constant a, and e_{33} and e_{31} are the piezoelectric coefficients. The polarization induced by a shear strain related to the piezoelectric tensor, e_{15}, will be ignored in this study.

VI. Results and Discussion

The parameters of the calculations are shown in Table 1. In this section, The results of boron-containing QD structure were presented, and they grouping depending on their QD layer structure.

A. BGaN structures

Figure 1 shows the TE and TM gain modes for $BGaN/AlN$ at some boron mole fractions. The TE spectra are higher than that of TM by three orders. All the spectra are peaked at 199nm. Reducing x (boron)-mole fraction by one order increases the gain by three orders. The spontaneous emission spectra are a picture of the gain spectra. High TE (and TM) is of central importance in LED applications compared to its QW counterpart and promising in UV QD LED.

Figure 2 shows the possibility of increasing spectra by more reduction in the boron mole-fraction. The QD spectra are still at the same peak wavelength despite the change of mole fraction, which refers to the main effect of the AlN barrier that has a wide bandgap as a comparison with to that of QD.

Figure 3 shows the polarization effect of $BGaN/AlN$ QD structure. At 0.15 boron mole-fraction, the pizoelectric polarization changes from positive to negative due to strain effect at this mole fraction. Note that, works (and this work) are not go this fraction [2].

Figure 4 studies $BGaN/BAlN$ QD structure. It shows the effect of adding boron to the barrier layer. A few boron mole fractions in the barrier still give similar results when the AlN alone is the barrier in both spectrum height at wavelength. Higher boron content in the barrier reduces the spectrum.

In Figure 5, AlGaN have been examined as a barrier layer for BGaN QD structure. However, BGaN emits at 199nm at all of the above structures, Figure 5 shows the increasing peak gain and a slight blue shift with increasing Al-mole fraction in the barrier layer of BGaN/AlGaN QD structure attributed to the wider bandgap of AlN, which controls the transitions. Al-barrier controlling of the emission wavelength is also with other QD structures not containing boron [20].

B. BAlGaN structures

Figure 6 examines $BAlGaN/AlGaN$ QD structure and shows the possibility of increasing gain by reducing boron mole-fraction. TE gain is increased by one order while TM mode is doubling.

Figure 7 shows the effect of Al composition on the QD layer in $BAlGaN/AlN$ QD structure. Increasing Al content reduces the spectra. Increasing the Al content by 0.001 reduces the TE gain by three times. A similar result is also shown [2, 8] for BAlGaN QWs.

Figure 8 shows the polarization when adding a few Al mole-fraction. As comparison with Figure 3 (for $BGaN$), the spontaneous polarization was increased for the Al-containing structure, and then the total polarization is reduced for this structure which is preferred.

Figure 9 shows the $BAlGaN/BAlN$ QD structure at different boron content in the barrier layer where their emission wavelength is 200nm. Reducing the boron content (increasing Al) in the barrier increases the peak gain.

C. BInGaN structures

Figure 10 examines BInGaN/AlN QD structure. The effect of adding indium instead of aluminum exhibits a spectrum with a peak at the same wavelength. However, it becomes higher. BInGaN/AlN QD structure is increased by four orders in both TE and TM compared with BAlGaN/AlN QD structure in Figure 6. Figure 11 shows the polarization of BInGaN, which is not different from BAlGaN.

In addition to exploring the boron-based QD structures in the UV region, BInGaN/AlGaN is examined in Figure 12 and shows interesting results. Adding Ga to the AlN barrier changes the emission wavelength from 199 into 290nm with a high TE gain while absorption for TM mode under few reductions of boron content in the QD.

Continuing examination of the AlGaN barrier, Figure 13 shows the emitted wavelength is made shorter with the increasing of boron in the QD, which is also shown in [2, 8, 11] for QWs due to growing bandgap with boron composition [21].

In both figures 12 and 13, the gain changes from positive to negative, i.e., gain due to high transparency point of these structures which means that a high carrier density must be used to attain gain.

Figure 14 shows an increment in the absolute value of polarization for BInGaN/AlGaN compared with BInGaN/AlN QD structures.

Then, the research has examined the addition of boron to the barrier layer. Figure 15 shows BInGaN/BAlN QD structure where the structure emits near 222nm by controlling boron composition in the barrier. Better TE and TM gain values are obtaining.
Figure 16 gives another example of the BInGaN/BALN QD structure emitting possibility, which emits near 235nm by adjusting boron content in the QD and barrier layers. Reducing boron fraction reduces gain.

VII. Conclusions

Boron-based QD structures emit at ultraviolet were examined theoretically. Ternary and quaternary lattice matched structure: $BGaN/AlN$, $BGaN/BAlN$, $BGaN/AlGaN$, $BAlGaN/BAlN$, $BInGaN/AlN$, $BInGaN/AlGaN$, and $BInGaN/BAlN$. TE and TM gain spectra, spontaneous emission, spontaneous polarization, and piezoelectric polarization were experienced in these structures, and high spectra result from reducing boron content. The total polarization is few at 0.15 boron mole-fraction. Binary systems were emitted at 199nm. Higher boron content in the barrier reduces the spectrum. $BInGaN/AlN$ spectrum was increased by four orders compared to the corresponding Al structure. $BInGaN/BAlN$ was emitted near 222nm by controlling boron in the barrier with good TE and TM gain. $BInAlN/BGaN$. The structure $BInGaN/BAlN$ can have a peak wavelength near 235nm. Elongating wavelength to 290nm is possible with $BInGaN/AlGaN$ with high yield appearing at few boron.

Disclosers: The authors declare that there is no conflict of interest.

TABLE I. THE PARAMETERS USED IN THE CALCULATIONS [2, 12, 20].

Parameters	BN	GaN	AlN	InN
E_g (eV) at T= 300 K	5.2	3.44	6.25	0.64
m_e/m_0 at T= 300 K	0.752	0.2	0.32	0.07
m_{hh}/m_0 at T= 300 K	0.88	1.4	3.53	1.63
a (Å) at T = 300 K	2.534	3.189	3.112	3.545
e_{31} (C/m^2)	0.27	-0.49	-0.6	-0.57
e_{33} (C/m^2)	-0.85	0.73	1.46	0.97
C_{13} (10^{11} dyne/cm^2)	7.4	9.4	12.7	12.7
C_{33} (10^{11} dyne/cm^2)	107.7	20.0	38.2	38.2
P_{sp}(C/m^2)	-2.174	-0.034	-0.090	-0.042
Δ_{cr}(eV)	0.333	0.010	-0.169	0.040
Δ_{so}(eV)	0.21	0.017	0.019	0.005

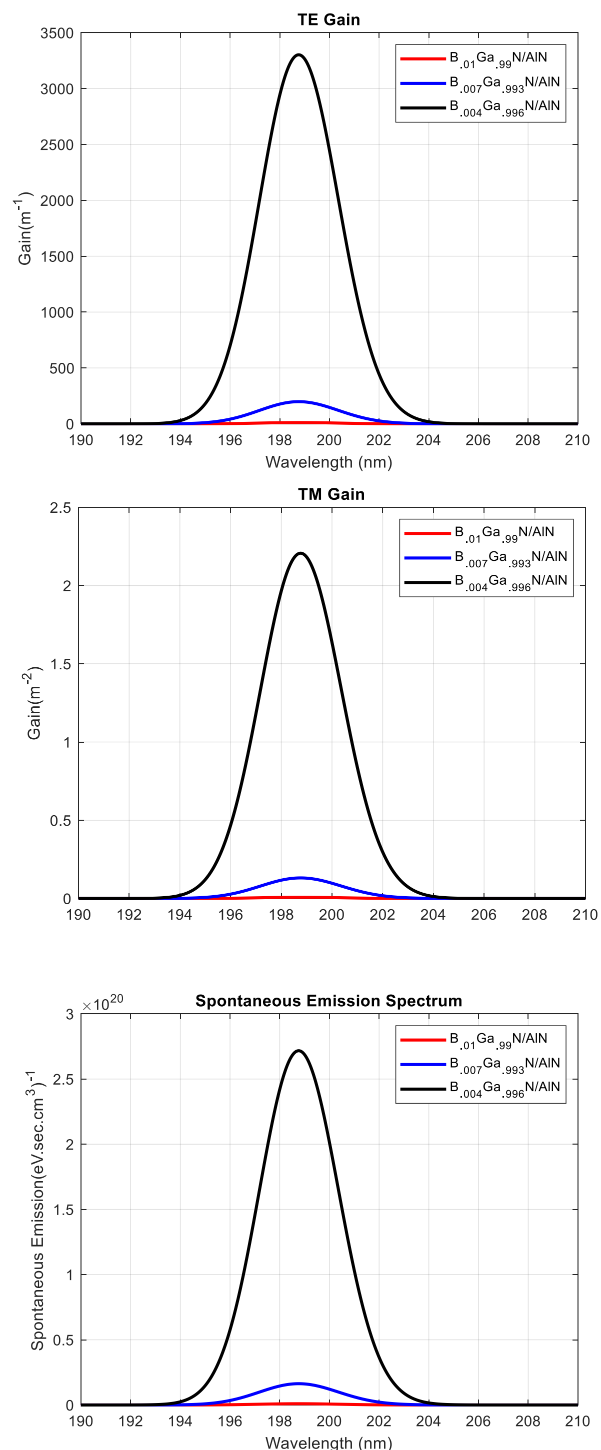

FIGURE 1: THE TE AND TM GAIN MODES AND SPONTANEOUS EMISSION FOR $BGaN/AlN$ QD STRUCTURE.

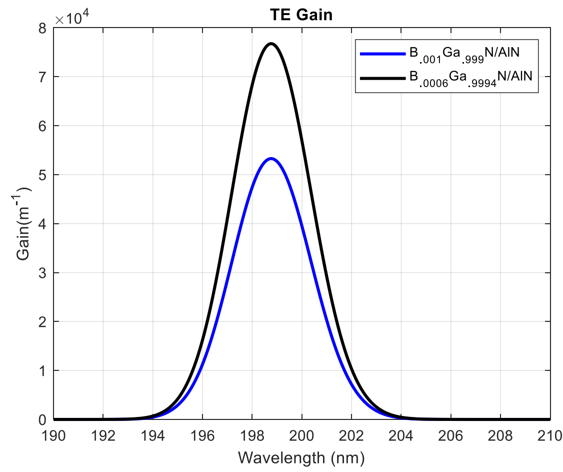

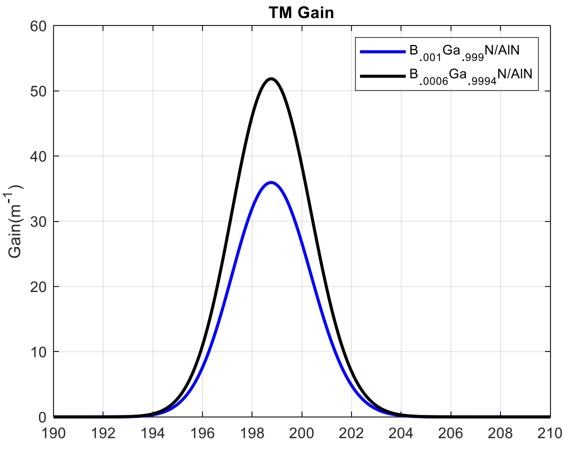

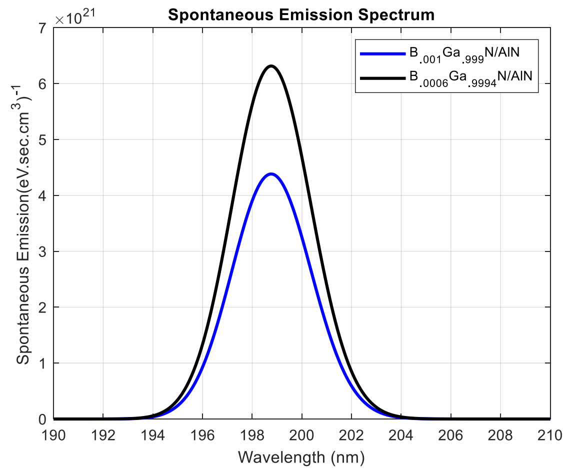

FIGURE 2: THE TE AND TM GAIN MODES AND SPONTANEOUS EMISSION FOR $BGaN/AlN$ QD STRUCTURE UNDER SMALL BORON CONTENT.

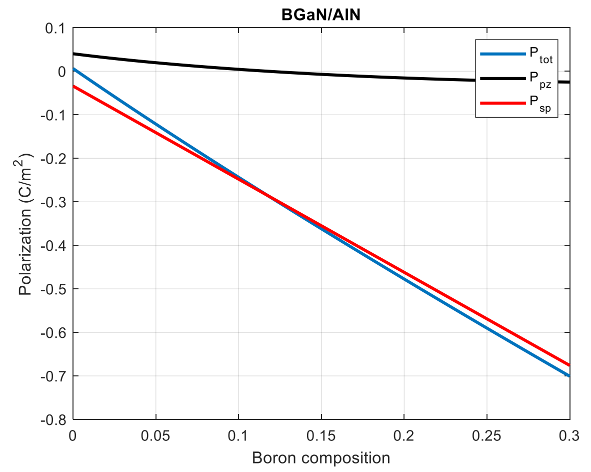

FIGURE 3: THE POLARIZATION COMPONENTS FOR $BGaN/AlN$ QD STRUCTURE.

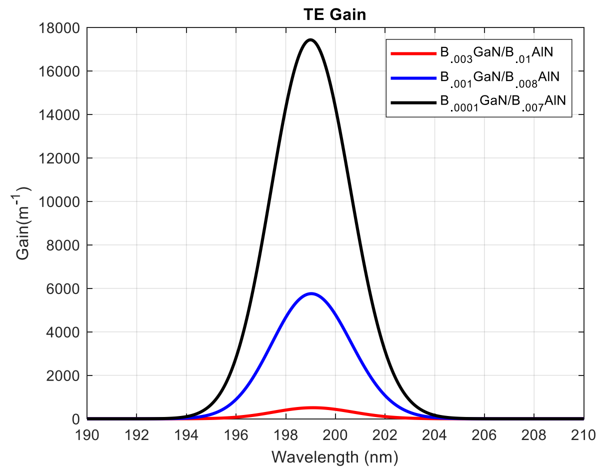

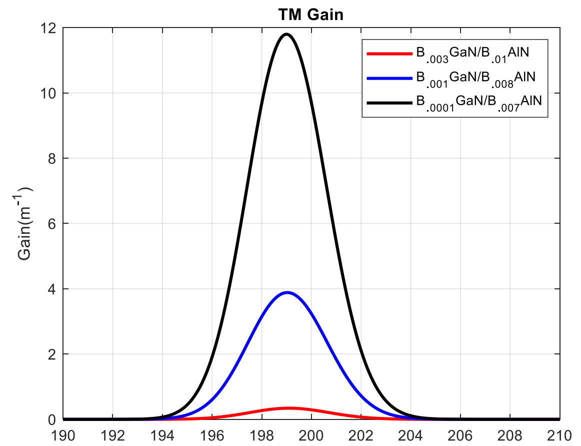

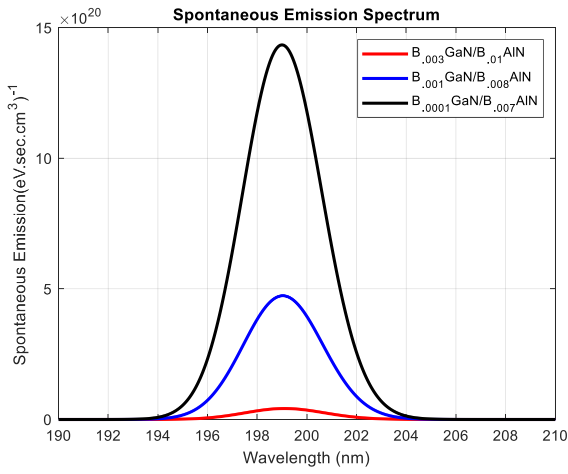

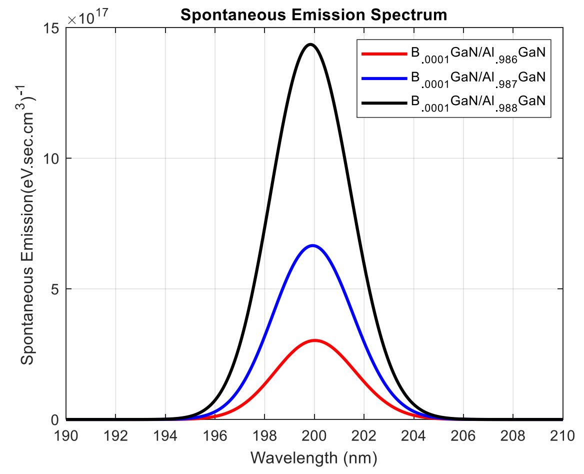

FIGURE 4: THE TE AND TM GAIN MODES AND SPONTANEOUS EMISSION FOR $BGaN/BAlN$ QD STRUCTURE.

FIGURE 5: THE TE AND TM GAIN MODES AND SPONTANEOUS EMISSION FOR $BGaN/AlGaN$ QD STRUCTURE.

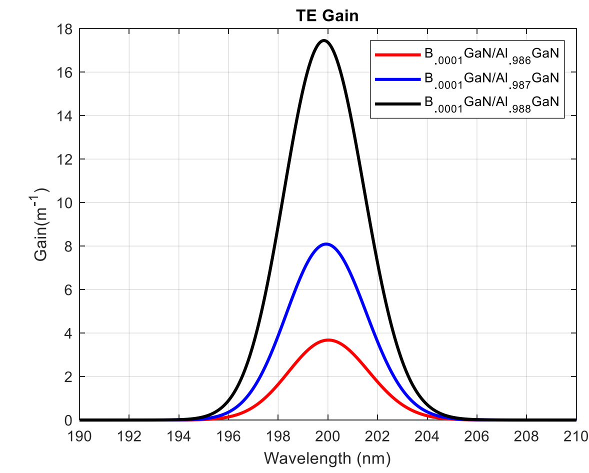

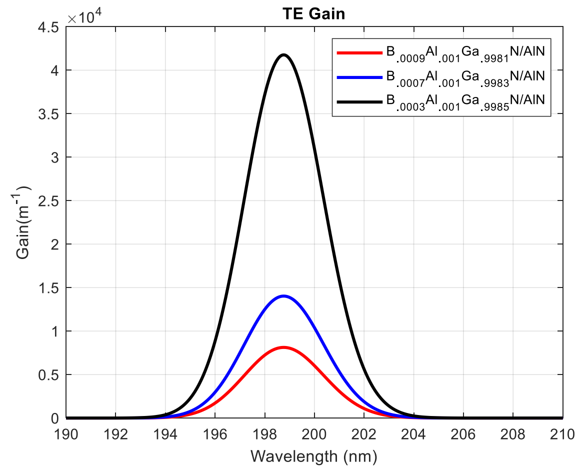

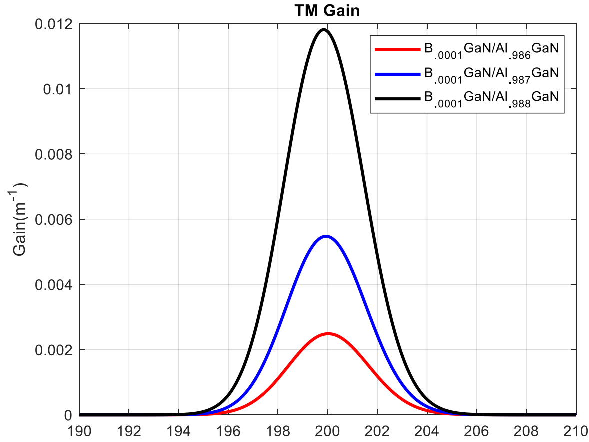

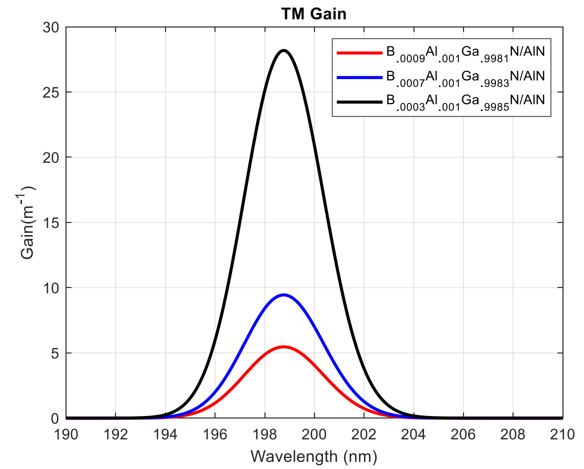

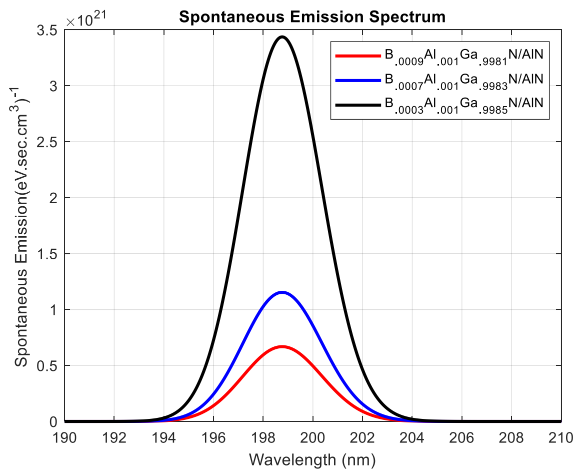

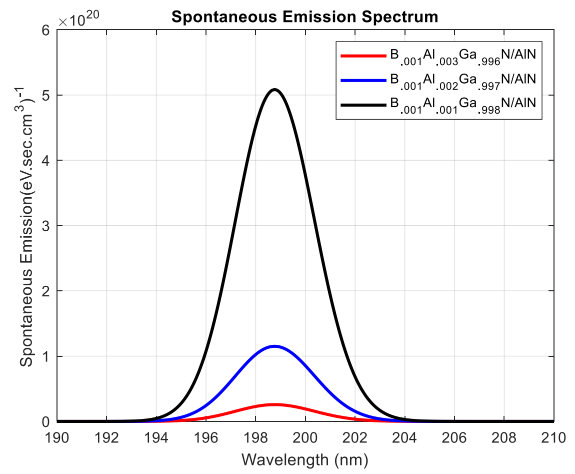

FIGURE 6: THE TE AND TM GAIN MODES AND SPONTANEOUS EMISSION FOR $BAlGaN/AlN$ QD STRUCTURE.

FIGURE 7: THE TE AND TM GAIN MODES AND SPONTANEOUS EMISSION FOR $BAlGaN/AlN$ QD STRUCTURE.

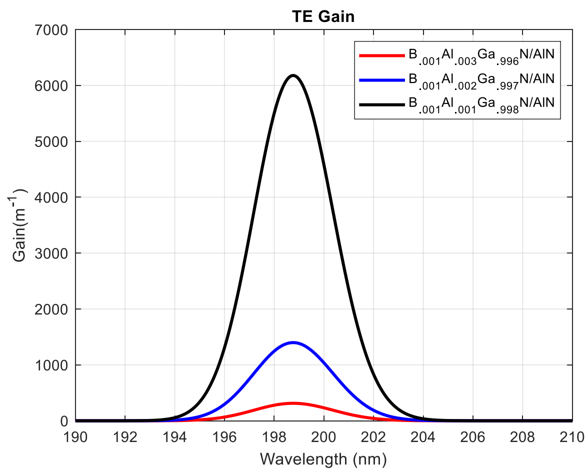

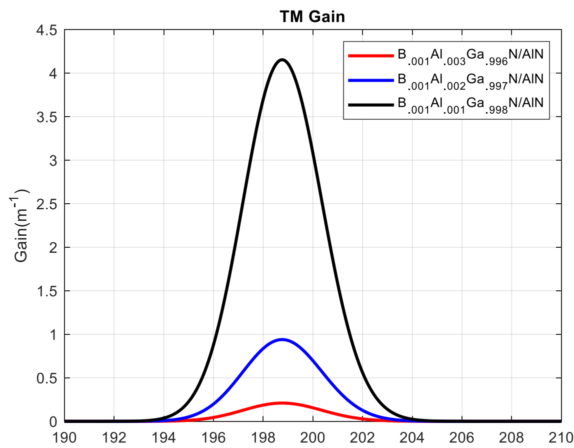

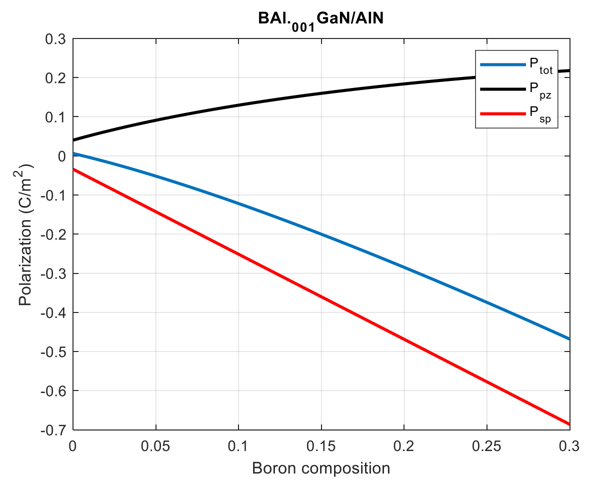

FIGURE 8: THE POLARIZATION COMPONENTS FOR $BAlGaN/AlN$ QD STRUCTURE.

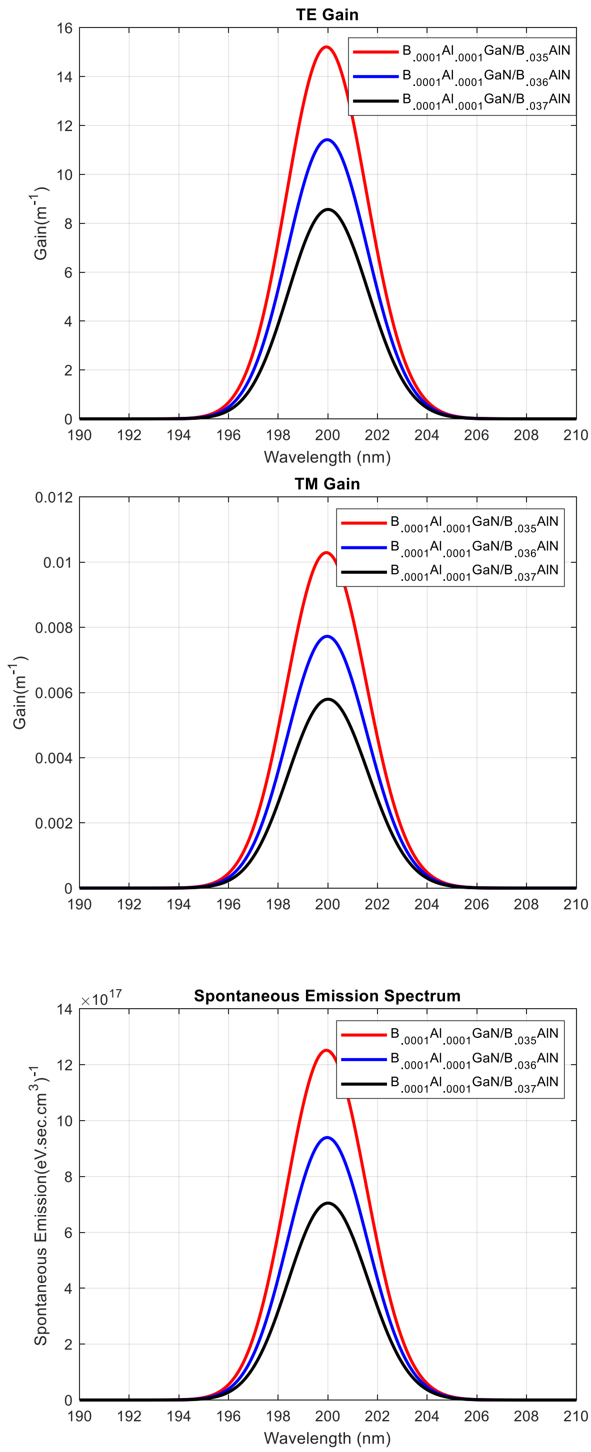

Figure 9: The TE and TM gain modes and spontaneous emission for $BAlGaN/BAlN$ QD structure.

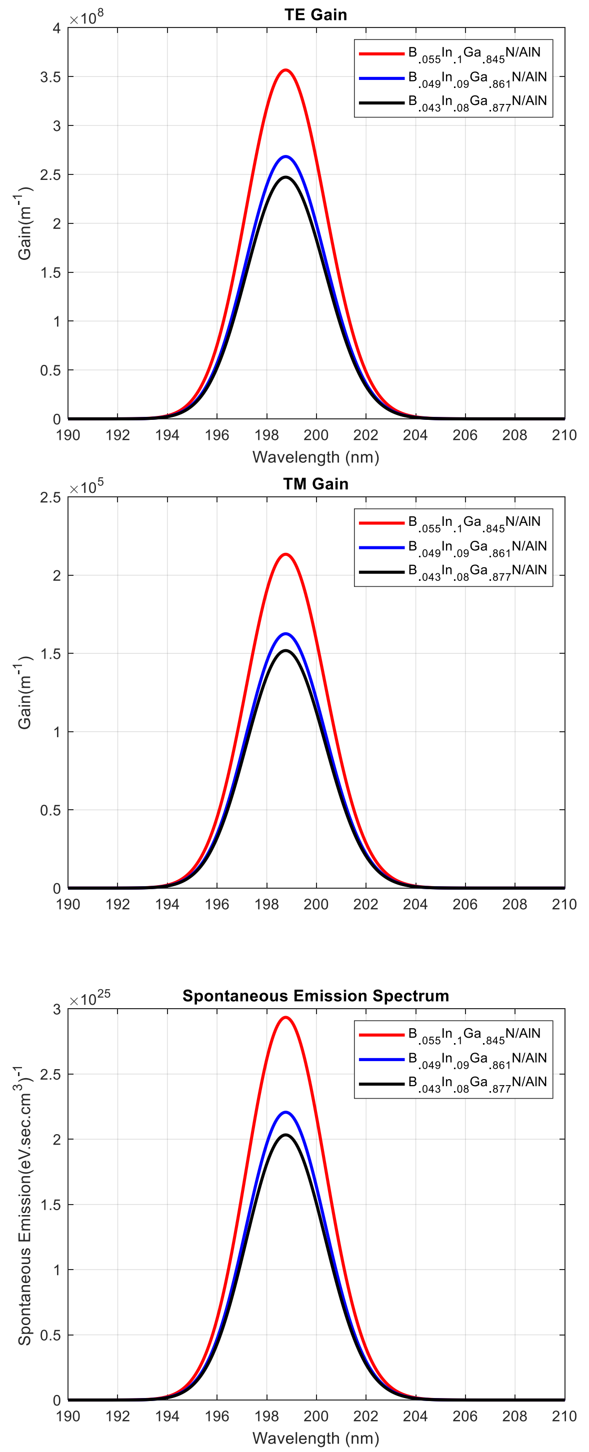

Figure 10: The TE and TM gain modes and spontaneous emission for $BInGaN/AlN$ QD structure.

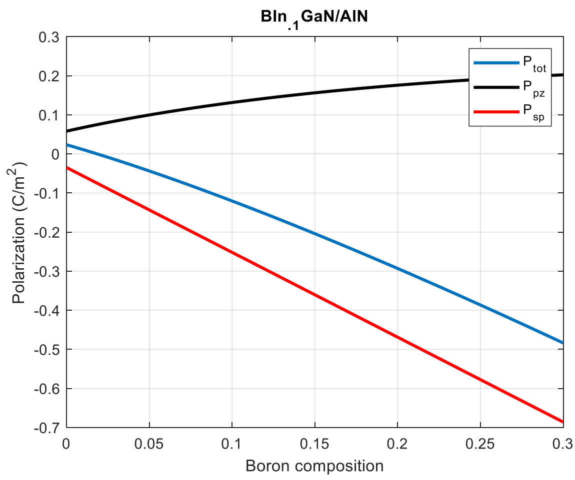

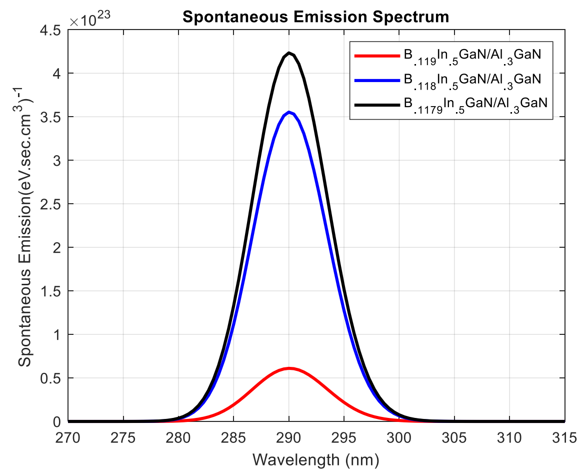

FIGURE 11: THE POLARIZATION COMPONENTS FOR $BAlGaN/AlN$ QD STRUCTURE.

FIGURE 12: THE TE AND TM GAIN MODES AND SPONTANEOUS EMISSION FOR $BInGaN/AlN$ QD STRUCTURE AT DIFFERENT BORON COMPOSITIONS.

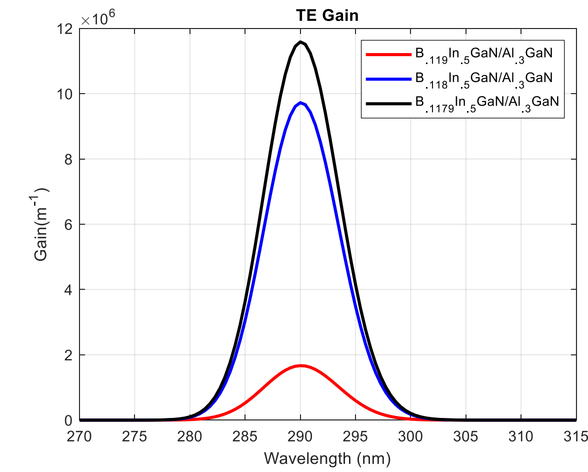

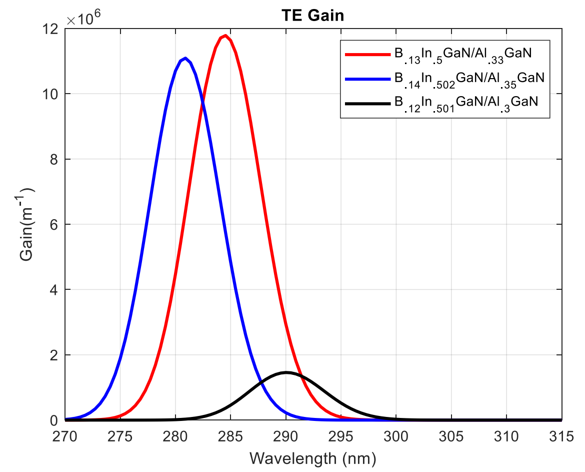

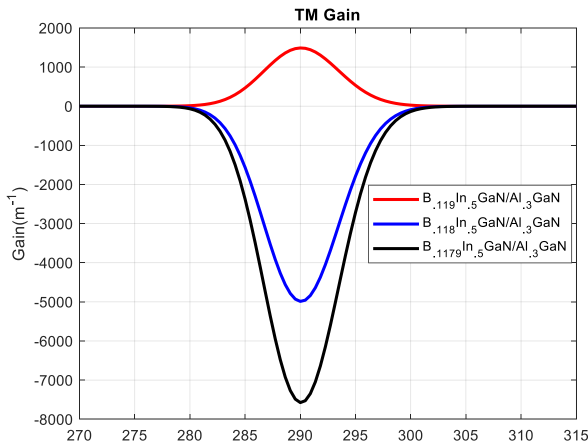

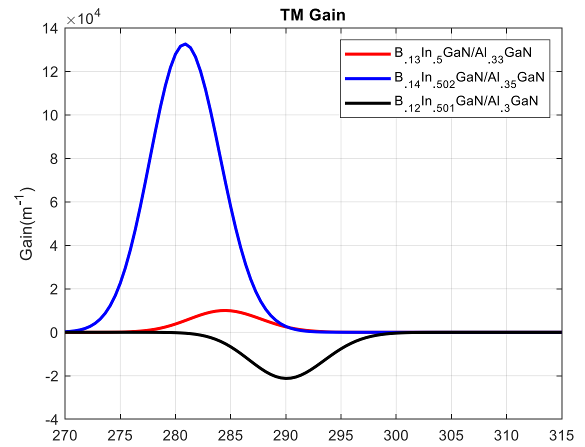

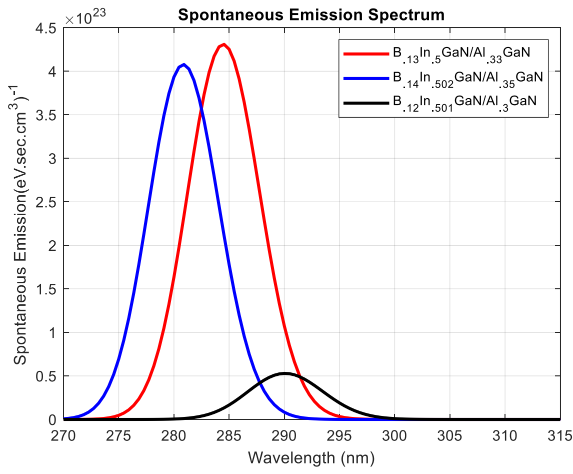

FIGURE 13: THE TE AND TM GAIN MODES AND SPONTANEOUS EMISSION FOR $BInGaN/AlGaN$ QD STRUCTURE.

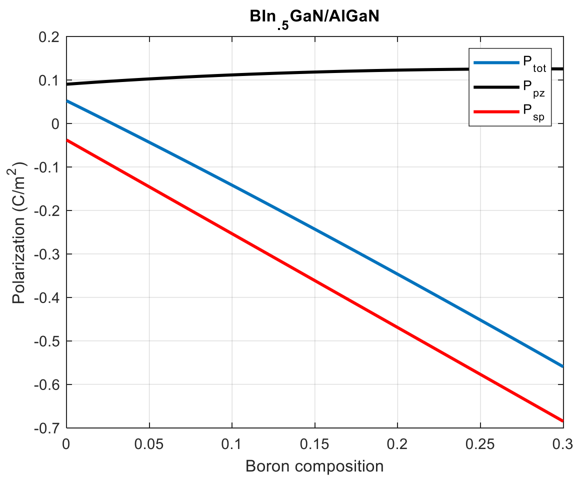

FIGURE 14: THE POLARIZATION COMPONENTS FOR $BInGaN/AlGaN$ QD STRUCTURE.

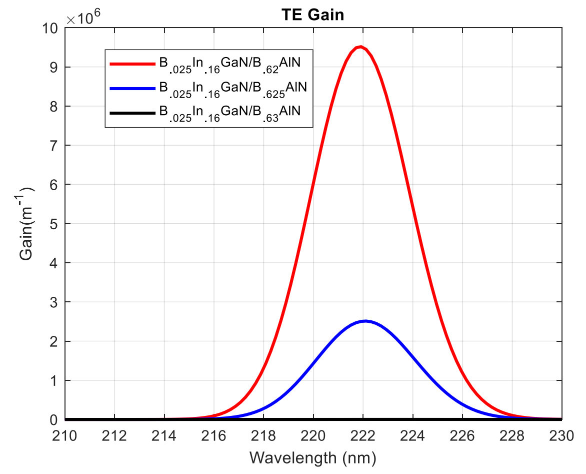

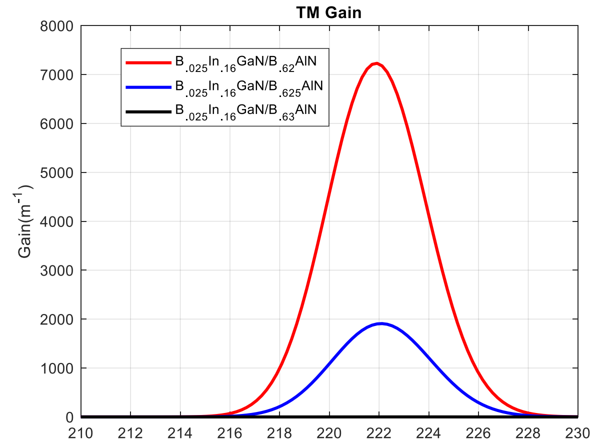

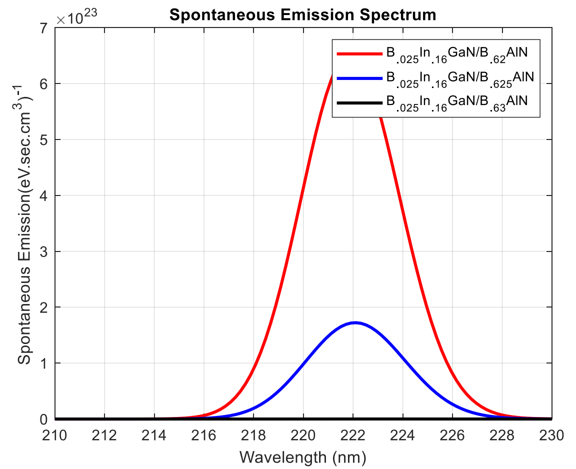

FIGURE 15: THE TE AND TM GAIN MODES AND SPONTANEOUS EMISSION FOR $BInGaN/BAlN$ QD STRUCTURE.

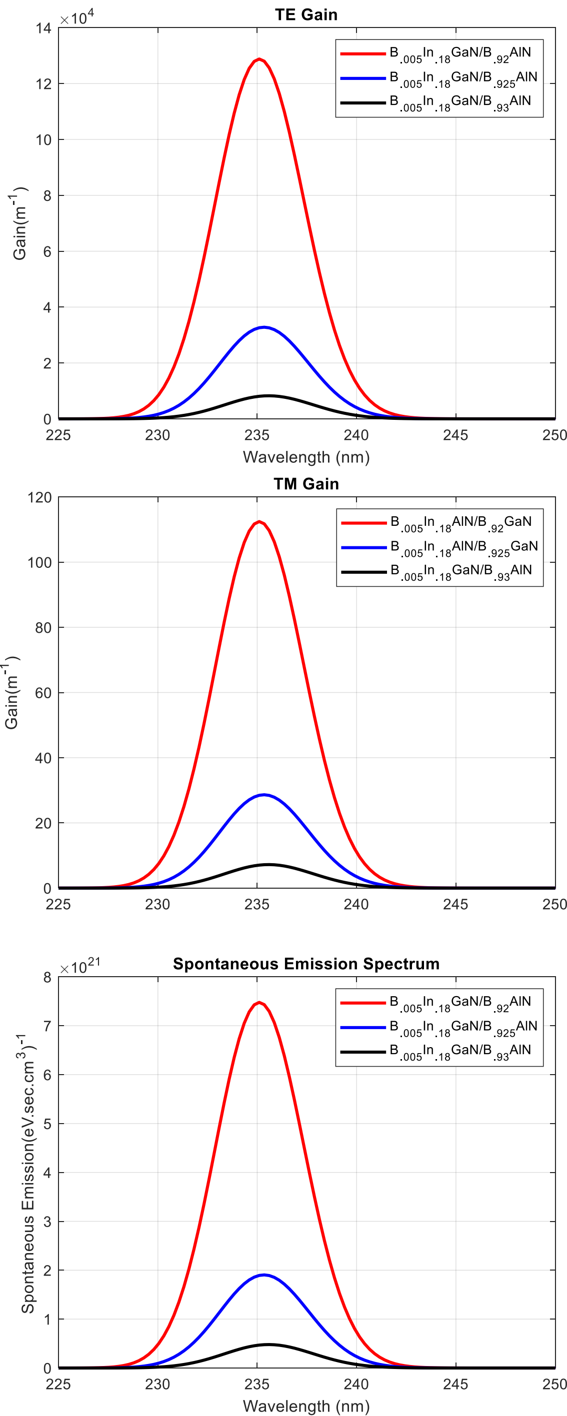

FIGURE 16: THE TE AND TM GAIN MODES AND SPONTANEOUS EMISSION FOR $BInGaN/BAlN$ QD STRUCTURE EMITTING AROUND 235NM.

REFERENCES

[1] G. Rajauria and B. K. Tiwari, Eds., Fruit Juices Extraction, Composition, Quality and Analysis, 464 Ch.24: Short-Wave Ultraviolet Light Inactivation, (2018) Elsevier Inc.

[2] S.-H. Park, "High-efficiency BAlGaN/AlN quantum well structures for optoelectronic applications in ultraviolet spectral region", Optics Express 23 (2015) 3623-29.

[3] S.-H. Park and D. Ahn, "Effect of boron incorporation on light emission characteristics of UV BAlGaN/AlN quantum well structures", Applied Physics Express 9 (2016) 021001.

[4] A. Erdmann, Optical and EUV Lithography: A Modeling Perspective, (2021) SPIE.

[5] C. Zhang, S. Divitt, Q. Fan, W. Zhu, A. Agrawal, Y. Lu, T. Xu, and H. J. Lezec, "Low-loss metasurface optics down to the deep ultraviolet region", Light: Science & Applications 9 (2020).

[6] S.-H. Park and D. Ahn, "Lattice-matched double dip-shaped BAlGaN/AlN quantum well structures for ultraviolet light emission devices", Superlattices and Microstructures 117 (2018) 413-417.

[7] S.-H. Park, D. Ahn, and S. L. Chuang, "Electronic and optical properties of a-and m-plane wurtzite InGaN–GaN quantum wells", IEEE J. Quantum Electron.

43(2007) 1175-82.

[8] S.-H. Park and D. Ahn, "Theoretical Studies on TM-Polarized Light Emission for Ultraviolet BAlGaN/AlN Optoelectronic Devices", IEEE PHOTONICS TECHNOLOGY LETTERS 28 (2016) 2153-55.

[9] D. Y. Kim, J. H. Park, J. W. Lee, S. Hwang, S. J. Oh, J. Kim, C. Sone, E. F. Schubert, and J. K. Kim, "Overcoming the fundamental light-extraction efficiency limitations of deep ultraviolet light-emitting diodes by utilizing transverse-magnetic-dominant emission," Light, Sci. Appl. 4 (2015) e263.

[10] T. KIMURA_ and T. Matsuoka, “Calculation of Phase Separation in Wurtzite $In_{1-x-y-z}Ga_xAl_yB_zN$ ", Japanese J. Applied Physics 46 (2007) L574–L576.

[11] S.-H. Park, W.-P. Hong, and J.-J. Kim, "Comparison of optical properties of polarization-matched c-plane and lattice-matched a-plane BInGaN/GaN quantum well structures", Physica B: Condensed Matter 570 (2019) 94–99.

[12] S. L. Chuang, Physics of photonic devices, 2nd Ed. Wiley (2009).

[13] J. Kim and S. L. Chuang, "Theoretical and Experimental study of optical gain, refractive index change and linewidth enhancement factor of p-doped Quantum-Dot Lasers", IEEE J. Quantum Electronics 42, 942-952 (2006).

[14] R. A. Arif, H. Zhao, Y.-K. Ee, and N. Tansu, "Spontaneous Emission and Characteristics of Staggered InGaN Quantum-Well Light-Emitting Diodes", IEEE J. Quantum Electron. 44 (2008) 573-580.

[15] S. L. Chuang, “Optical Gain of Strained Wurtzite GaN Quantum-Well Lasers”, IEEE J. Quantum Electron. 32 (1996) 1791-1800.

[16] D. Bimberg, N. Kirstaedter, N. N. Ledentsov, Zh. I. Alferov, P. S. Kop’ev, and V. M. Ustinov, "InGaAs–GaAs Quantum-Dot Lasers", IEEE J. Selected Topics Quantum Electronics 3, 196-205 (1997).

[17] M. Asada, Y. Miyamoto, Y. Suematsu, "Gain and the threshold of three-dimensional quantum-box lasers", IEEE J. Quantum Electron 22 (1986)1915–1921.

[18] J. N. Jabir, S. M. M. Ameen, and A. H. Al-Khursan, "Plasmonic quantum dot nanolaser: effect of "waveguide Fermi energy", Plasmonic 14 (2019) 1881-1891.

[19] O. Ambacher, R. Dimitrov, M. Stutzmann, B. E. Foutz, M. J. Murphy, J. A. Smar, J. R. Shealy, N. G. Weimann, K. Chu, M. Chumbes, B. Green, A. J. Sierakowski, W. J. Schaff, and L. F. Eastman, "Role of Spontaneous and Piezoelectric Polarization Induced Effects in Group-III Nitride Based Heterostructures and Devices", Phys. Stat. Sol. (b) 216 (1999) 381.

[20] B. Al-Nashy and Amin H. Al-Khursan, "Linear and Nonlinear Gain of Sb-based Quantum-Dot Semiconductor Optical Amplifiers", Recent Patents on Electrical Engineering 3 (2010) 232-240.

[21] T. Honda, M. Tsubamoto, Y. Kuga, and H. Kawanishi, "Optical Gain in BGaN Lattice-Matched to (0001) 6H-SiC", Mat. Res. Soc. Symp. Proc., Materials Research Society 482 (1998) 1125-1129.